Smart Structures and Systems, *Vol. 31*, *No. 2* (*2023*) *141-154*
https://doi.org/10.12989/sss.2023.31.2.141

Feasibility study on using crowdsourced smartphones to estimate buildings' natural frequencies during earthquakes

Ting-Yu Hsu*, Yi-Wen Ke [b], Yo-Ming Hsieh [a] and Chi-Ting Weng [c]

Department of Civil and Construction Engineering, National Taiwan University of Science and Technology, Taipei 10607, Taiwan

(*Received April 3, 2022, Revised October 15, 2022, Accepted October 29, 2022*)

Abstract. After an earthquake, information regarding potential damage to buildings close to the epicenter is very important during the initial emergency response. This study proposes the use of crowdsourced measured acceleration response data collected from smartphones located within buildings to perform system identification of building structures during earthquake excitations, and the feasibility of the proposed approach is studied. The principal advantage of using crowdsourced smartphone data is the potential to determine the condition of millions of buildings without incurring hardware, installation, and long-term maintenance costs. This study's goal is to assess the feasibility of identifying the lowest fundamental natural frequencies of buildings without knowing the orientations and precise locations of the crowds' smartphones in advance. Both input-output and output-only identification methods are used to identify the lowest fundamental natural frequencies of numerical finite element models of a real building structure. The effects of time synchronization and the orientation alignment between nearby smartphones on the identification results are discussed, and the proposed approach's performance is verified using large-scale shake table tests of a scaled steel building. The presented results illustrate the potential of using crowdsourced smartphone data with the proposed approach to identify the lowest fundamental natural frequencies of building structures, information that should be valuable in making emergency response decisions.

Keywords: crowdsourcing; fundamental natural frequency; orientation alignment; post-earthquake building safety; smartphones

1. Introduction

Ensuring prompt and effective emergency responses is essential for improving the earthquake resilience of cities against major earthquakes, and having prompt information regarding potential structural damage to affected buildings would be particularly useful during the initial emergency response. Currently, initial emergency responses are based on the estimated number of damaged buildings within a region, which is determined by using the observed peak ground acceleration, as well as relevant fragility curves and building information data, such as data regarding building materials, numbers of stories, structural systems, ages, etc., for the region in question (FEMA).

For buildings equipped with structural health monitoring systems utilizing accelerometers, data loggers, and computers with appropriate analysis programs, the damage states of individual buildings can be estimated based on the measured acceleration response during an earthquake. However, due to high installation and maintenance costs, only some buildings are equipped with such systems, even though relatively low-cost sensor networks (Clayton *et al*. 2015, Finzi Neto *et al*. 2010, Kohler *et al*. 2016, Hsu *et al*. 2018, Lei *et al*. 2020), wireless sensor networks (Zonta *et al*. 2010, Haque *et al*. 2015, Sun *et al*. 2015, 2017, Kim *et al*. 2016a, b, Shen *et al*. 2021), and camera-based sensor networks (Dong *et al*. 2019, Yu *et al*. 2019, Hsu *et al*. 2020) have been proposed for monitoring structural health.

The ability of smartphones to measure accelerations has been demonstrated in numerous studies (Dashti *et al*. 2014, Feng *et al*. 2015, Kong *et al*. 2016a), hence the time history of the measured accelerations will not be shown in this study for conciseness. Moreover, the natural frequencies of cables on a cable-stayed bridge (Yu *et al*. 2015), a bridge's operational frequencies (Elhattab *et al*. 2019, Shrestha *et al*. 2018), and a building's fundamental frequencies (Kong *et al*. 2018) have been successfully identified with acceptable accuracy using the acceleration data measured by smartphones. Similarly, another study found that the mode shapes of a pedestrian link bridge could be identified using smartphones if synchronous data from high-quality accelerometers were utilized as a reference (Ozer *et al*. 2015). It is important to note, however, that while smartphones are normally carried by human beings, these past studies effectively utilized the phones as deployed sensors – that is, the researchers designated the locations and orientations of the phones during the measurements made by the phones.

Typically, at any given time, some portion of the smartphones possessed by members of the general public

*Corresponding author, Ph.D., Associate Professor,
E-mail: tyhsu@ntust.edu.tw
[a] Ph.D. Associate Professor
[b] MS
[c] Research Assistant

ISSN: 1738-1584 (Print), 1738-1991 (Online)

are physically immobile, e.g., those left sitting on a desk or table, and could thus be utilized as portable seismometers for the detection of earthquakes. Relatedly, some researchers have attempted to employ smartphone-based crowdsourcing approaches for earthquake early warning purposes (Faulkner *et al*. 2014, Finazzi 2016, Kong *et al*. 2016b, Hsu and Nieh 2020), with some studies finding that smartphones can be used to predict the intensity of an upcoming earthquake after a trigger has been classified as an earthquake event (Kong *et al*. 2016a, Hsu and Nieh 2020).

An example of successful smartphone-based crowdsourcing application is MyShake. Over 335,000 people around the globe have installed the app until 2016 and more than 900 earthquakes have been detected by the app (Kong *et al*. 2016a). Therefore, keep the crowds' smartphones measuring vibration signals and denote their data continually become possible based on the success of the MyShake app. If numerous smartphones are distributed within a building, some of them can be used to collect the building's seismic vibration response, which in turn makes it possible to assess the building's post-earthquake safety. In a previous study, Hsu *et al*. (2022) proposed using crowdsourced smartphone data collected from physically immobile smartphones to estimate the inter-story drift ratios of buildings during earthquakes. However, in order to obtain the precise locations of the smartphones and the building information necessary for damage estimation, e.g., the structural types, numbers of stories, story heights, and seismic design levels of the buildings, Bluetooth-beacon-equipped products must be available in the buildings, a requirement that limits the application of the proposed approach.

In this study, therefore, we propose the use of a smartphone-based crowdsourcing approach for estimating the lowest fundamental natural frequencies of buildings during earthquakes that does not require assistance from Bluetooth-beacon-equipped products to determine the precise locations of the smartphones, and the feasibility of the proposed approach is studied. This approach, if effective, would thus enable the lowest fundamental natural frequencies of a large number of buildings to be quickly collected for improved earthquake emgency responses without the deployment of costly structural health monitoring systems in the buildings. The methodology through which crowdsourced smartphone data are used to estimate buildings' lowest fundamental natural frequencies is explained in the next section. Next, a numerical study performed to verify the proposed algorithm is described. Then, following the presentation of an experimental study utilizing the proposed approach, a discussion and conclusions are presented in the final section.

2. Methodology

In order to explain the procedures employed in using crowdsourced smartphone data to identify the lowest fundamental natural frequencies of buildings during earthquakes, a flow chart of the procedures is shown in Fig. 1. The first two procedures have already been developed and utilized in earthquake early warning systems (Hsu and Nieh 2020), while the third and fourth procedures have already been developed and utilized in a previous study (Hsu *et al*. 2022); hence, only a brief introduction of the these procedures is provided here. In the present study, we investigated whether, by using the smartphone application developed for the study, crowdsourced smartphone data collected from physically immobile smartphones can effectively be harnessed to estimate the lowest fundamental natural frequency of a given building without knowing the precise locations and orientations of the smartphones. Relatedly, it should be noted that, in this study, only smartphones lying horizontally were regarded as being in

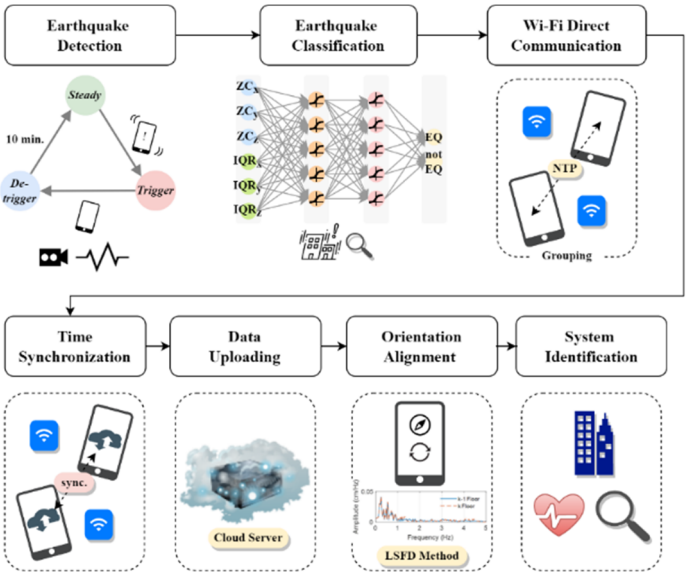

Fig. 1 Flow chart of the procedures employed in utilizing crowdsourced smartphone data to identify the fundamental natural frequencies of buildings during earthquakes

a stable (i.e., physically immobile) state. In addition, the sampling frequency of the smartphones of different brands in this study are all 50 Hz. If the sampling frequency is larger than 50 Hz, e.g., 100 Hz, then the measured data can be resampled to 50 Hz in real-time first and then be applied to the proposed procedures.

The detection of an earthquake event itself is the first procedure in the overall process. To accomplish that, the short-term average/long-term average (STA/LTA) algorithm (Withers *et al*. 1998), an algorithm frequently utilized for earthquake event detection in geoscience research, is used to trigger and de-trigger the crowdsourced smartphones, with the STA and LTA themselves defined as the averages of the root mean square of three acceleration component signals of, respectively, 20 and 500 points. The detail of the STA/LTA algorithm utilized in this study can be found in the following section of experimental study. When a given smartphone remains in a de-triggered state for longer than 10 minutes, it is defined as being in the "steady" state. Moreover, to ensure that accelerations are only measured by those smartphones that are lying horizontally, a given phone is not regarded as being in the steady state if the absolute value of the pitch or roll angles of the phone's gyroscope is greater than 5°. Relatedly, the triggering of a phone will only be regarded as indicative of a possible earthquake event when the phone has been triggered after having been in the steady state, in which case the acceleration signals between the triggering and de-triggering caused by the event will be recorded. As such, mere vibrations of the crowdsourced smartphones resulting from their being moved by their owners will not be recorded.

The next procedure in the overall process consists of determining whether or not the recorded acceleration signals are actually the result of an earthquake event. To meet that objective, earthquake classifiers are obtained using the artificial neural network (ANN) approach, with the resulting ANN classifiers consisting of a single hidden layer of five neurons with a sigmoid activation function and a single output and the input features utilized consisting of the interquartile range (IQR) between the 25th and 75th percentiles of the acceleration vector sum of the three-component acceleration and the zero-crossing (ZC) rate of the highest value component. As previously demonstrated by Hsu and Nieh (2020), high levels of classification accuracy can be obtained using the ANN approach (2020). In order to reduce the possibility of missing an earthquake, a total of 10 ANN classifiers are employed. Each ANN classifier utilizes the features of N seconds after a trigger with N starting between one second to ten seconds after the trigger. The trigger event will be classified as an earthquake once it is classified as an earthquake at any second after the trigger using the corresponding ANN classifier.

The third procedure in the overall process, which consists of using Wi-Fi Direct technology (https://www.wi-fi.org/discover-wi-fi/wi-fi-direct) to establish a wireless connection between nearby smartphones, is then applied only to those events that are classified as earthquake events. This procedure enables the crowdsourced phones to both identify peer devices nearby and establish a direct wireless link to them without the use of an intermediate Wi-Fi access point. Furthermore, two given smartphones can then communicate with one another at typical Wi-Fi speeds following the establishment of the direct wireless link.

Synchronizing the connected smartphones is the fourth procedure in the overall process. This step is required because while every smartphone has a built-in clock, each clock may be insufficiently accurate due to drift stemming from a lack of regular updates from the Internet time servers. More specfically, past studies have shown that smartphones updated through early (Miškinis *et al*. 2011) and 5G (Borenius *et al*. 2019) mobile networks can have, respectively, hundreds and tens of milliseconds of error even when the standard time synchronization mechanism referred to as the network time protocol (NTP) is utilized. We therefore employ the NTP mechanism (Mills 1991) to the crowdsourced phones through the Wi-Fi Direct link to synchronize the time at which the acceleration signals are recorded. The accuracy of the algorithm has previously been verified as acceptable through a validation test in which the estimated time delay between each pair of smartphones was only 0.00458 s on average within the frequency range of 0.1 to 25 Hz (Hsu *et al*. 2022).

Performing an orientation alignment of the crowdsourced smartphones is the fifth procedure in the overall process. While most smartphones contain a magnetometer, the accuracy levels of the orientations determined by these built-in magnetometers are not sufficiently accurate enough, particularly those that occur during earthquake excitations. Relatedly, Hsu *et al*. (2022) previously proposed using the least Fourier spectrum difference (LFSD) method to provide the necessary orientation alignment in the frequency domain. More specifically, while the LFSD method was originally used to align the orientations of smartphones on two adjacent floors, it is employed in the current study to align the orientations of any two of the crowdsourced smartphones. It should be noted, relatedly, that because only those smartphones determined to be lying in a steady, horizontal state are used in this study, only the horizontal orientation (azimuth angle) is used in determining the orientation alignment. It is assumed, furthermore, that the Fourier spectra of the acceleration data measured in the two horizontal components are distinct and, therefore, that the pattern of the Fourier spectra will be altered as the orientations of the smartphones change. When the orientations of two smartphones are identical, the difference between their Fourier spectra $\Delta U_k\left(\omega_j,\theta\right)$ in both horizontal components, defined as Eq. (1), should be very small

$$\begin{aligned}\Delta U_k^x\left(\omega_j,\theta\right)&=\left|U_k^x\left(\omega_j,\theta\right)-U_r^x\left(\omega_j\right)\right|\\ \Delta U_k^y\left(\omega_j,\theta\right)&=\left|U_k^y\left(\omega_j,\theta\right)-U_r^y\left(\omega_j\right)\right|\end{aligned}\tag{1}$$

in which U_k^x represents the Fourier spectrum of the k-th smartphone's local in x-direction, and ω_j represents the jth discrete frequency. U_r^x represents the Fourier spectrum of the reference smartphone, which can be selected randomly from the available smartphones. The Fourier spectra of the k-th smartphone at orientation θ are calculated as

$$U_k^x(\omega_j,\theta) = U_k^x(\omega_j)cos\theta + U_k^y(\omega_j)sin\theta$$
$$U_k^y(\omega_j,\theta) = -U_k^x(\omega_j)sin\theta + U_k^y(\omega_j)cos\theta \quad (2)$$

The summation of the Fourier spectra difference $\Delta U_k\ (\theta)$ is calculated as

$$\Delta U_k\ (\theta) = \sum_{j=1}^{M}\left(\Delta U_k^x(\omega_j,\theta) + \Delta U_k^y(\omega_j,\theta)\right) \quad (3)$$

in which M represents the total number of discrete frequencies considered. The orientation of the k-th smartphone, θ, will rotate at an interval of $\Delta\theta$, and it begins from the initial orientation of the smartphone. The orientation with the smallest value of $\Delta U_k\ (\theta)$ is then selected as the best estimation of the orientation, denoted as θ_B. In a previous study, Hsu *et al*. (2022) recommended using $\Delta\theta = 1°$ for practical applications to save computational effort in crowdsourced smartphones.

There are two types of LFSD methods, i.e., Type I and Type II. Type I employs the amplitude of the Fourier spectrum when calculating Eq. (1), while Type II employs the complex value, which means that Type II considers not only the amplitude but also the phase of the Fourier spectrum values. The results of these two types under different conditions will be discussed in the numerical study.

The last procedure in the overall process consists of performing system identification of the building in question using the acceleration data uploaded by the smartphones to estimate the lowest fundamental natural frequency of the building. We assume that the smartphones are widely spread throughout and sufficient in number in a given building; hence, all the acceleration responses of each floor, including the lowest floor, are measured. Two well-established and popular output-only system identification algorithms, i.e., frequency domain decomposition (FDD; e.g., Brincker *et al*. 2001) and stochastic subspace identification (SSI; e.g., Peeters and De Roeck 1999), are employed to perform system identification when the ground excitation is not available, e.g., when, in spite of the ground excitation being measured, it is not known which smartphones are located on the ground floor. If the ground excitation is available, however, then input-output system identification algorithms can be used. We consider two algorithms, i.e., the frequency response function (FRF; e.g., Ewins 2000) and combined deterministic and stochastic system identification (CSI; e.g., Reynders and De Roeck 2008) algorithms, in this study. Because these algorithms are well-known, the details of these algorithms are ommitted from this paper to ensure conciseness.

3. Numerical study

A finite element model of an eight-story reinforced concrete (RC) building with a one-story basement was constructed, as shown in Fig. 2. The story height of every story except the basement was 3.65 m, while that of the basement was 3.95 m, resulting in a total height of 33.2 m. The other dimensions of each story were 35.4 m (X) × 59.6 m (Y). The fundamental natural frequencies of the X-direction, Y-direction, and Z-rotation were 1.771 Hz, 1.494 Hz, and 2.558 Hz, respectively.

The linear elastic earthquake responses of the building with a 5% damping ratio when excited during 17 earthquakes simulated using the ETABS commercial software were studied. Data for the 17 earthquakes were collected from the Significant Earthquakes Database provided by the United States Geological Survey (USGS) and the Consortium of Organizations for Strong Motion Observation Systems (COSMOS), as well as from the strong earthquakes database provided by the Taiwan Strong Motion Instrumentation Program (TSMIP), with the relevant data being shown in Table 1. The acceleration responses of five locations on each floor, i.e., the Center, Corner A, Corner B, Corner C, and Corner D locations, were assumed to be measured during the simulated seismic excitations, as shown in Fig. 3.

The crowdsourced smartphones are assumed to be placed horizontally on the floor or on rigid pieces of furniture within each story of the building; hence, only the structural response and ground excitation during the excitations are measured. The target natural frequency to be identified is the lowest fundamental natural frequency. It is

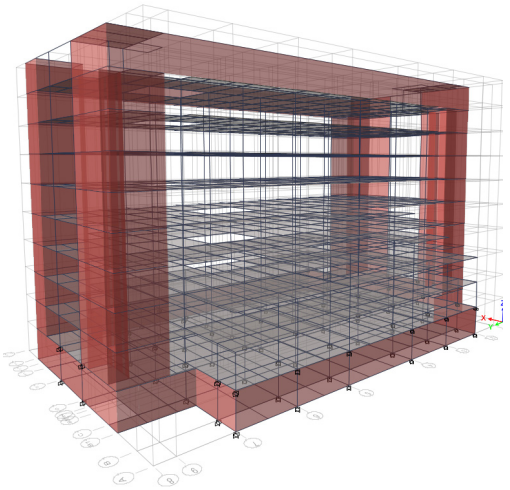

Fig. 2 Numerical model of the eight-story RC building

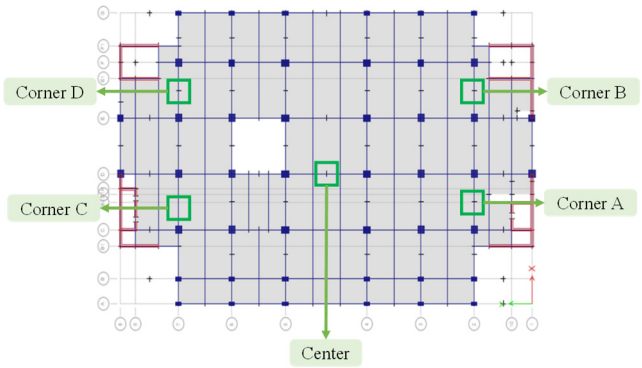

Fig. 3 Numerical model of the eight-story RC building

Table 1 The 17 earthquakes considered in the numerical study

Earthquake	Region	Station	Date	M	PGA
El Centro	US/CA	USGS station 0117	1940/05/19	6.9	342
Taft	US/CA	USGS station 1095	1952/07/21	7.5	176
India-Burma Border	India	IITR station berl	1988/08/06	7.2	337
Loma Prieta (Cptl.)	US/CA	CSMIP station 47125	1989/10/18	7.0	463
Northridge (Van)	US/CA	CSMIP station 24386	1994/01/17	6.7	445
Kobe	Japan	CUE station	1995/01/16	6.9	500
Northwest China	China	CSB station 19001	1997/04/11	6.1	294
Chi Chi	Taiwan	TCU084	1999/09/21	7.6	985
Hector Mine	US/CA	USGS station 5075	1999/10/16	7.1	59
Lefkada	Greece	Lefkada No1	2003/08/14	6.3	417
Wenchuan	China	051WCW	2008/05/12	8.0	958
Samoa Islands	Samoa	Afiamalu	2009/09/29	8.0	93
Meinong	Taiwan	CHY098	2016/02/05	5.0	192
Puebla	Mexico	UNAM	2017/09/19	7.1	54
Hualien	Taiwan	ENA	2018/02/06	6.2	428
Anchorage	US/CA	Rabbit Creek	2018/11/30	7.0	652

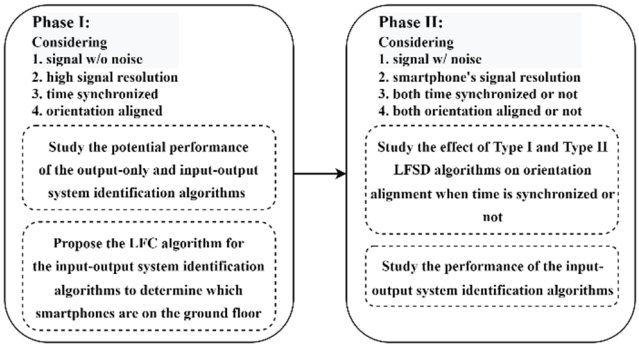

Fig. 4 The flowchart of the numerical study

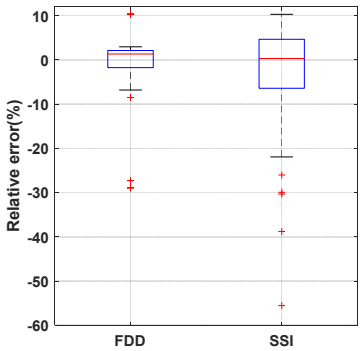

Fig. 5 The boxplots of the relative errors of the estimated lowest fundamental natural frequency when using the FDD and SSI output-only algorithms

assumed that the natural frequency will become lower due to damage and that the maximum frequency variation due to environmental and operational condition changes is approximately 10% (Wu *et al*. 2017). Hence, only the frequency range between 0.1 Hz and 1.1 times the value of the lowest fundamental natural frequency, i.e., 1.1 × 1.494 = 1.643 Hz, are considered in the analysis. Because when the lowest fundamental frequency of the building becomes lower than 0.1 Hz, it is already too soft. Before the frequency reaches this limit, i.e., 0.1 Hz, the building should have already collapsed. Hence, 0.1 Hz should be low enough to be the lower limit.

The flowchart of the procedures in the numerical study is shown in Fig. 4. In the Phase I of the numerical study, the potential performance of the output-only and input-output system identification algorithms under relatively ideal conditions is studied; hence, no noise is measured and there are no time differences or orientation differences between the smartphones. It is assumed the longitudinal and translational directions of the smartphones are in X- and Y-directions of the building, respectively. The acceleration time histories of the smartphones at one of the five locations on each floor between the triggering and de-triggering during each excitation are treated as one dataset to estimate the lowest fundamental natural frequency; hence, 85 datasets (5 locations × 17 excitations) are analyzed for each algorithm.

The boxplots of the relative errors of the estimated lowest fundamental natural frequency when using the FDD and SSI output-only algorithms are shown in Fig. 5. Generally, the relative errors of the SSI algorithm are much larger than those of the FDD algorithm. However, the root-mean-square errors (RMSE) of the SSI and FDD algorithms are 8.2% and 11.8%, respectively, while the maximum relative errors of the SSI and FDD algorithms are 28.9% and 55.6%, respectively. The accuracy of the estimated lowest fundamental natural frequency when using the output-only algorithms therefore seems unacceptable, even under the aforementioned relatively ideal conditions.

The main reasons for the large errors of the estimated lowest fundamental natural frequency when using the output-only algorithms were either (a) the frequency

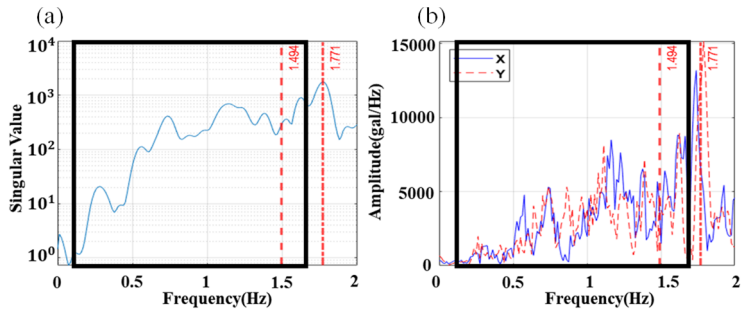

Fig. 6 (a) The singular value of the FDD algorithm, and (b) the Fourier spectrum of the input excitation of a typical case in which the frequency content of the input excitation around 1.771 Hz is larger than the frequency content around 1.494 Hz

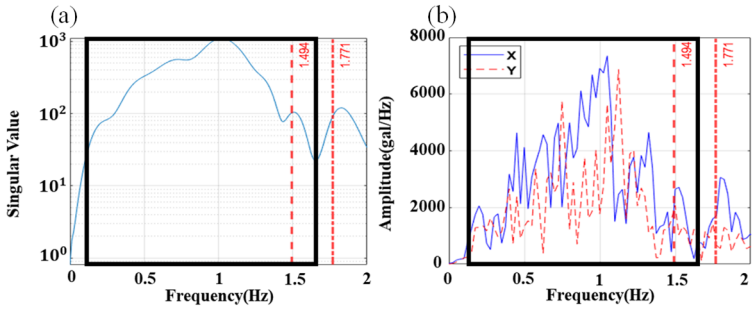

Fig. 7 (a) The singular value of the FDD algorithm, and (b) the Fourier spectrum of the input excitation of a typical case in which the frequency content of the input excitation around 10 Hz is larger than the frequency content around 1.494 Hz

content of excitation at the frequencies close to the other natural frequencies being larger or (b) the frequency content of excitation at the frequencies lower than the lowest fundamental natural frequency being much larger. A typical example of the first reason when using the FDD algorithm is shown in Fig. 6. In Fig. 6(b), the frequency content around the natural frequency of 1.771 Hz, which is marked by the vertical dash-dotted line, is larger than the frequency content of the lowest fundamental natural frequency of 1.494 Hz, which is marked using the vertical dashed line. Because only the frequency range between 0.1 Hz and 1.643 Hz is considered in the analysis, as indicated by the thick black rectangular box, the largest singular value of 1.643 Hz in Fig. 6(a) is selected. A typical example of the second reason for the large errors when using the FDD algorithm is shown in Fig. 7. In Fig. 7(b), the frequency content around 1 Hz is much larger than the frequency content close to the natural frequencies of 1.1494 Hz and 1.771 Hz; hence, the largest singular value of 1.10 Hz in Fig. 7(a) is selected.

The boxplots of the relative errors of the estimated lowest fundamental natural frequency when using the CSI and FRF input-output algorithms are shown in Fig. 8. Note that when using the FRF algorithm, the estimated frequency could be different when using the measured accelerations on different floors as the output. Hence, the final estimated lowest fundamental natural frequency when using the FRF algorithm is obtained using the average estimated frequency of all the floors as the output after the outliers of the estimated frequency are excluded. Generally, the relative errors of the CSI algorithm are smaller than those of the

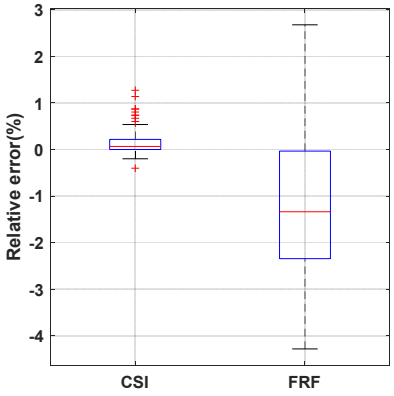

Fig. 8 The boxplots of the relative errors of the estimated lowest fundamental natural frequency when using the CSI and FRF input-output algorithms

FRF algorithm. The RMSE of the CSI and FRF algorithms are only 0.3% and 2.0%, respectively, while the maximum relative errors of the CSI and FRF algorithms are 1.2% and 4.3%, respectively. Evidently, the accuracy of the estimated lowest fundamental natural frequency when using the input-output algorithms seems quite acceptable. As a result, in the following study, only the input-output algorithms are employed.

That said, the above results are obtained when the input ground excitations are measured and known. However, when using crowdsourced smartphones, even though we assume that the input ground excitations are measured, we still do not know which smartphones are located on the

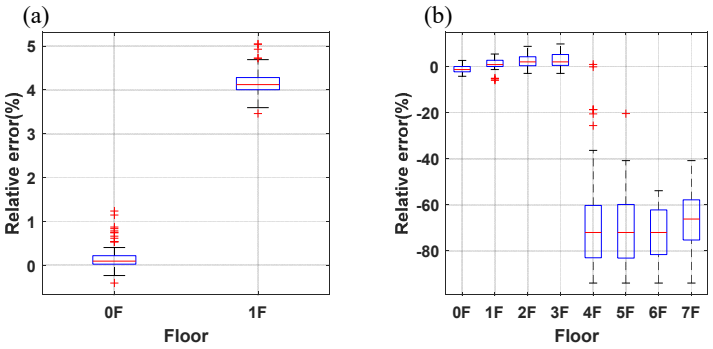

Fig. 9 The boxplots of the relative errors of the estimated lowest fundamental natural frequency when using the CSI and FRF input-output algorithms and when smartphones on floors other than the ground floor or basement level are mistakenly used as the input excitations

ground floor or basement level. Relatedly, the boxplots of the relative errors of the estimated lowest fundamental natural frequency when using the CSI and FRF input-output algorithms, and when the smartphones on floors other than the ground floor or basement level are mistakenly used as the input excitations, are shown in Figs. 9(a) and (b), respectively. When using the CSI algorithm, the relative error when using the smartphones on the 1st floor as the input is approximately 4%, while the relative error when using the smartphones on the 2nd to the 7th floors as the input is not shown because no reasonable frequency is successfully identified. As for using the FRF algorithm, the relative errors when using the smartphones on the 1st floor, 2nd floor, and 3rd floor as the input are relatively small, but the reletive errors when using the smartphones on the higher floors as the input are extremely large, approximately 70%.

As a result, it is concluded that the estimated lowest fundamental natural frequency is not reliable if using arbitrary smartphones as the input. Therefore, we propose the least frequency content (LFC) algorithm to determine which smartphones are on the ground floor or basement level based on the measured acceleration data. Because the transmissibility between the ground input acceleration and the floor response acceleration is larger than 1.0 around the frequency of the lowest fundamental natural frequency, the accelerations measured on the ground floor should be smaller than those measured on the other floors. The frequency content E is calculated as

$$E = \sum_{i=1}^{N} (|X(f_i)| + |Y(f_i)|) \tag{4}$$

where X and Y are the fast Fourier transforms of the two horizontal measured accelerations at discrete frequency f_i, and N is the total number of discrete frequencies considered. The frequency range considered in this study is between 0.1 Hz and 1.1 times the lowest fundamental natural frequency, i.e., 1.643 Hz. When the orientation is correctly aligned and the time is perfectly synchronized for all the smartphones on the different floors, the ground floor determined by the proposed LFC algorithm for all 85 datasets is correct. Hence, it is possible to identify which measured accelerations are the input ground excitations and should thus be used in the input-ouput system identification algorithms.

In the Phase II of the numerical study, more realistic situations are considered in the following numerical study. More specifically, we consider the noise floor and resolution of the acceleration signals of the crowdsourced smartphones. Also, it is possible that time synchronization could be impossible if the Wi-Fi Direct link fails; hence, the times at which different smartphones recordthe acceleration signals could be different.

The standard deviations of the noise signals, i.e., noise floors, and acceleration resolutions of the smartphones released from 2014-2016 were approximately 3.38 cm/s^2 (gal) and 3.80 cm/s^2, respectively, at maximum (Hsu and Nieh 2020). It seems, therefore, that the quality of smartphones is increasing rapidly, as the average noise floor and acceleration resolution of the smartphones released from 2017-2019 became approximately 0.90 cm/s^2 and 0.48 cm/s^2, respectively, at maximum (Hsu *et al*. 2022). Hence, the original acceleration records were artificially contaminated with the noise of a noise floor of 1.0 cm/s^2 and then the resolution was changed to 0.5 cm/s^2 to simulate a possible realistic situation when applying the proposed approach.

Because the noise was added randomly, the time window between the trigger and de-trigger of each acceleration time history was different. If the signal recording times were synchronized, the intersection of all the acceleration time histories of the different floors would be truncated and used. As for the acceleration time histories without time synchronization, i.e., those with time asynchronization, the trigger times of the different floors were aligned, and then the time histories of shorter lengths were zero-padded to the same length of the longest one.

First, the effect of time synchronization on the performance when using the two types of LFSD methods for orientation alignment of any two smartphones is discussed. The longitudinal direction of the smartphone on the ground floor is assumed in the X-direction of the building, i.e., the orientation 0°. The orientation of the smartphones located on the 1st floor, 2nd floor, 3rd floor, and 4th floor is 30°, 60°, 90°, and 120°, respectively, and so on. Because the noise was added randomly, the results were

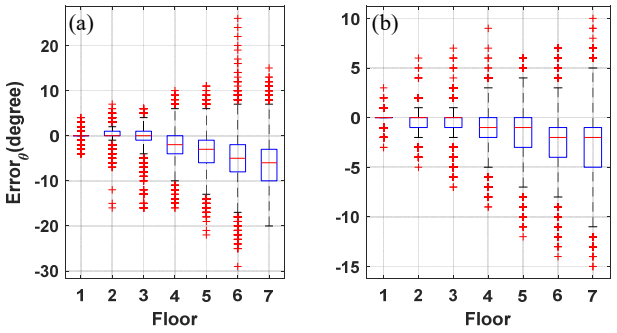

Fig. 10 Boxplots of the orientation alignment errors when the time is synchronized and when using the (a) Type I LFSD method; and (b) Type II LFSD method

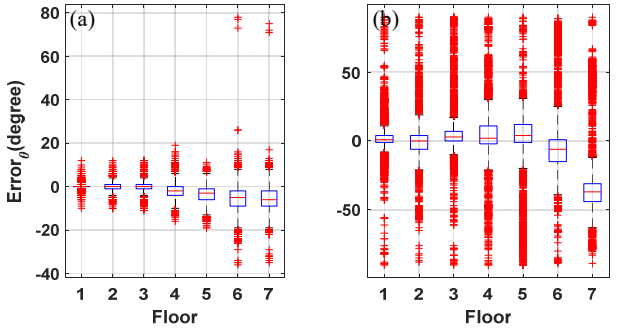

Fig. 11 Boxplots of the orientation alignment errors when the time is not synchronized and when using the (a) Type I LFSD method; and (b) Type II LFSD method

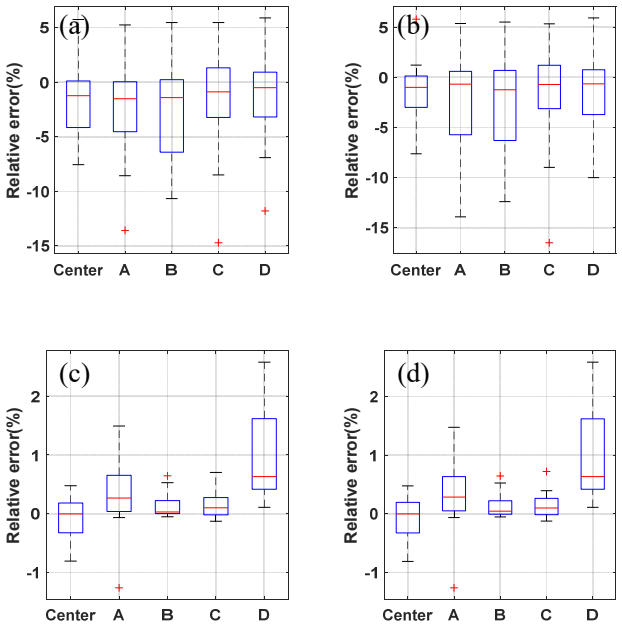

Fig. 12 The boxplots of the relative errors of the identified frequencies at five different locations when using the CSI algorithm: (a) asynchronized and without orientation alignment; (b) asynchronized and with orientation alignment; (c) synchronized and without orientation alignment; and (d) synchronized and with orientation alignment

different for each dataset. Hence, the results for 100 times of the 85 datasets were determined. Because the response accelerations on the structural floors contain the signals of structural characteristics, the frequency spectra of the measured accelerations should be similar, except for the input ground acceleration on the ground floor where almost no structural characteristic exists. Hence, when one of the smartphones is on the ground floor when performing orientation alignment using the LFSD method, the results are the worst, and are shown as a typical example herein.

When the time is synchronized, the RMSE of the orientations when using the Type I LFSD method is 4.8° and the maximum error is 29°, while the RMSE when using the Type II LFSD method is 2.8° and the maximum error is 15°, as shown in Fig. 10. However, when the time is not synchronized, the RMSE when using the Type I LFSD method is 22.6° and the maximum error is 78°, while the RMSE when using the Type II LFSD method is 2.8° and the maximum error is 90°, as shown in Fig. 11. In general, the error becomes larger as the floor becomes higher. This outcome is reasonable since the higher the floor, the more the response is dominated by the structural relative response but not the ground excitation, which is used as the reference in this typical example. Because the Type II LFSD method requires both the real and imaginary parts of the Fourier spectrum values, although the error is smaller when the time is synchronized, the error becomes much larger for the time asynchronization cases. On the other hand, because the Type I LFSD method only adopts the amplitude of the frequency spectrum, the error is smaller for the time asynchronization cases. Therefore, in the following study, the Type II LFSD method will be employed when the time is synchronized, and the Type I LFSD method will be used instead when the time is not synchronized.

Next, the effect of time synchronization and orientation alignment on the performance when using the CSI and FRF methods to estimate the lowest fundamental natural frequency is discussed. The ground floor was successfully identified when using the proposed LFC method for all the datasets. The boxplots of the relative errors of the identified frequencies at five different locations of all the datasets when using the CSI algorithm are shown in Fig. 12. The error when the time is synchronized and when using the CSI algorithm is always smaller than approximately 3%, either with or without the orientation alignment. This occurs because only the identified modal frequency, but not the identified mode shapes, is involved. However, if the time is not synchronized, the maximum relative error could reach approximately 17%.

Meanwhile, the boxplots of the relative errors of the identified frequencies at five different locations of all the datasets when using the FRF algorithm are shown in Fig. 13. The error when orientation alignment is performed and when using the FRF algorithm is always smaller than approximately 4%, either with or without time synchronization. This occurs because the FRF algorithm peaks the location of the lowest fundamental natural frequency in the frequency domain, in contrast with how the CSI algorithm deals with system identification in the time domain; hence, a small time-lag only slightly affects the

identified frequency when using the FRF algorithm. However, if orientation alignment is not performed, the maximum relative error could reach approximately 45%. This occurs because the frequency content of the accelerations along two horizontal axes will be mixed if no orientation alignment is performed. Note that during application, however, orientation alignment will always be performed, whether the time is synchronized or not. Based on these results, in the following study, the CSI algorithm is employed when the time is synchronized, and the FRF algorithm is employed when the time is not synchronized.

The aforementioned results shown in Figs. 10 and 11 indicate that error in the orientation still exists even after orientation alignment is performed when using the LFSD methods, and that the maximum error between the aligned angles could be 15° and 78° when the time is synchronized or not synchronized, respectively. Note that all eight floors are used together to estimate the lowest fundamental natural frequency when using the FRF algorithm, and although the maximum error of angle for a certain floor could be very large after the orientation alignment is performed, the errors of the other floors could still be quite small. Relatedly, when using the FRF algorithm, the outliers of the estimated lowest fundamental natural frequency will be excluded.

The boxplots of the relative errors of the identified frequencies when the smartphones are perfectly aligned, when using the FRF algorithm, and when time is synchronized or not synchronized are shown in Fig. 14. Compared to the results shown in Figs. 13(b) and (d), similar relative errors are obtained when the alignment is perfectly performed, i.e., when there is no angle error between the floors. It thus seems that the accuracy of the results after alignment when using the proposed LFSD algorithm already neared the accuracy of the results with perfectly aligned orientation.

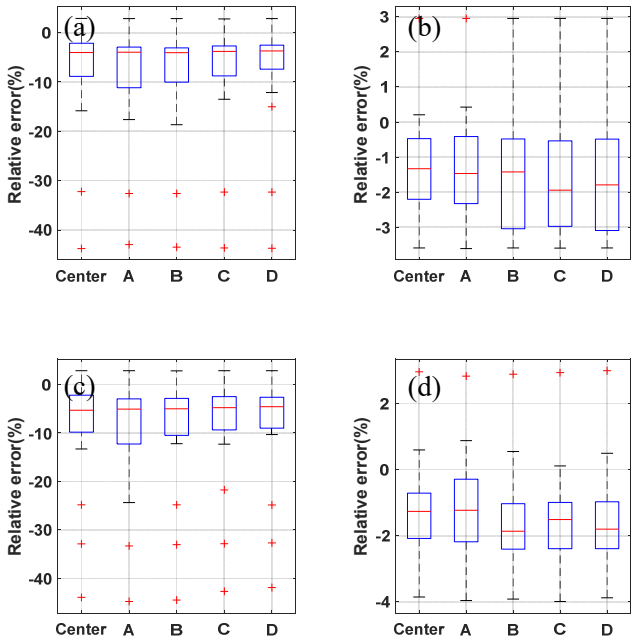

Fig. 13 The boxplots of the relative errors of the identified frequencies at five different locations when using the FRF algorithm: (a) asynchronized and without orientation alignment; (b) asynchronized and with orientation alignment; (c) synchronized and without orientation alignment; and (d) synchronized and with orientation alignment

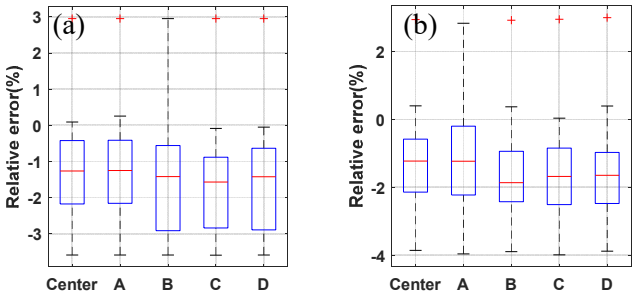

Fig. 14 The boxplots of the relative errors of the identified frequencies at five different locations when using the FRF algorithm, the smartphones are perfectly aligned, and (a) the time is not synchronized, and (b) the time is synchronized

4. Experimental study

In order to experimentally test the proposed system identification approach utilizing crowdsourced smartphone data, a scaled, four-story steel building structure was designed and constructed at the National Center for Research on Earthquake Engineering (NCREE) in Taiwan, as shown in Fig. 15. Each story of the structure was 2.0 m wide × 2.0 m deep × 2.0 m high. The additional mass of each floor was 2,000 kg, and the total mass of the whole structure was 15,194 kg. Each column and beam was made of A572Gr50 steel and had, respectively, an H-shaped cross-section of 150 × 150 × 7 × 10 mm and 125 × 60 × 6 × 8 mm. The weak axis of each column was along the global X-direction of the structure. The dimensions of the bottom of the columns on the first story were reduced to 150 × 50 ×

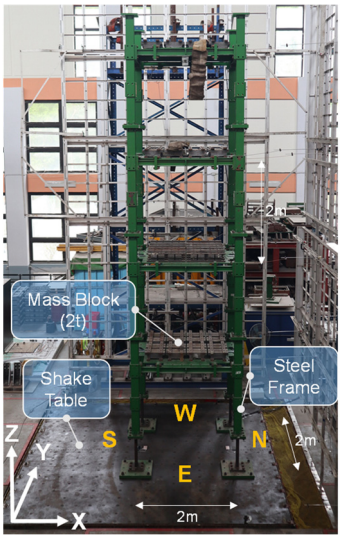

Fig. 15 The steel building structure on a shake table

Table 2 The 14 earthquake simulations applied during the shake table tests

No.	Earthquakes	Station	Axial	Scale	PGA (cm/s^2)
1	Hualien	HWA048	XYZ	10%	36
2	Meinong	CHY061	XYZ	10%	28
3	Chi Chi	TCU089	XYZ	10%	35
4	El Centro	USGS station 0117	XYZ	10%	46
5	Kobe	JMA station	XYZ	10%	99
6	Hualien	HWA048	XYZ	20%	72
7	Meinong	CHY061	XYZ	20%	56
8	Chi Chi	TCU089	XYZ	20%	69
9	El Centro	USGS station 0117	XYZ	20%	91
10	Kobe	JMA station	XYZ	20%	199
11	Hualien	HWA048	XYZ	30%	108
12	Meinong	CHY061	XYZ	30%	84
13	Chi Chi	TCU089	XYZ	30%	104
14	El Centro	USGS station 0117	XYZ	30%	137

7 × 10 mm to induce larger vibration responses for the experiment during the tests.

As shown in Table 2, excitations of the structure were achieved using simulations of five different earthquakes at scales of 10%, 20%, and 30%, with the exception of the 30% Kobe earthquake simulation due to safety considerations. More specifically, the 20% Kobe earthquake simulation induced a large nonlinear interstory drift, so it was thought that the larger 30% Kobe earthquake simulation could potentially cause the structure to collapse. As such, the 30% Kobe earthquake simulation was not applied. In total, therefore, 14 earthquake simulations were applied to the structure during the shake table tests, and their PGA values ranged between 28 and 199 cm/s^2, as shown in Table 2. Before the earthquake excitations, white noise excitation with a maximum amplitude of 30 gal, a frequency bandwith between 0.1 Hz and 50 Hz, and a duration of 50 s was conducted. The identified fundamental natural frequencies in the X and Y directions during the white noise excitation were 1.178 and 1.882 Hz, respectively.

As shown in Fig. 16, a Sharp Aquos Zero smartphone, Oppo A5 2020 smartphone, Sharp Aquos V smartphone, RealMe 5 smartphone, and Xiaomi Mi A3 smartphone were placed, respectively, on the ground floor, 1st floor, 2nd floor, 3rd floor, and 4th floor on the south side of the structure, while five Sharp Aquos V smartphones were placed on the north side of each floor. The smartphones are placed on the border simply because the center area is covered by the mass blocks, hence no space is available for the smartphones. Based on the results in the numerical study, the locations of the smartphones are not critical because only the lowest fundamental natural frequency is required to be identified. Unless the torsional natural frequency, which is usually not the lowest one, is required to be identified, the location on the border will be better than one in the center. As shown in Table 3, the average

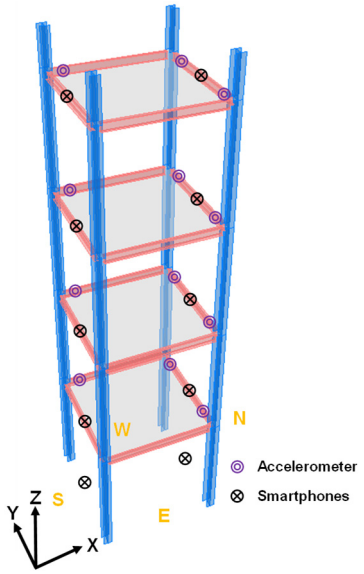

Fig. 16 The locations of the smartphones and accelerometers installed on each floor of the structure

Table 3 The smartphones used in the experimental study

Vendor	Model	Accelerometer Type	Noise Floor (cm/s^2)	Resolution (cm/s^2)	Release
Xiaomi	Mi A3	BMI160 Accelerometer	0.899	0.239	2019
OPPO	A5 2020	LSM6DS3C Accelerometer	0.468	0.120	2019
RealMe	RealMe 5	ICM4x6xx Accelerometer	0.390	0.479	2019
SHARP	AQUOS V	ICM40605 Accelerometer	0.576	0.119	2019
SHARP	AQUOS Zero	LSM6DSM Accelerometer	0.708	0.478	2019
Average			0.608	0.287	

noise floor and average resolution of the acceleration measurements of these smartphones were approximately 0.6 and 0.3 cm/s^2, respectively. Meanwhile, the orientations of the smartphones located on the ground floor, 1st floor, 2nd floor, 3rd floor, and 4th floor were 0°, 30°, 60°, 90°, and 120°, respectively. The typical arrangement of the orientation of each smartphone mounted on the 4th floor is shown in Fig. 17. Because a specific orientation was required for the smartphone placed on each floor during the experimental tests, in order to ensure that each smartphone was accurately oriented, double-sided tape was used to attach a transparent acrylic plate marked with datum lines on each floor. The given smartphone was then also attached to the acrylic plate via the double-sided tape in order to prevent the phone from sliding on the smooth surface of the acrylic plate. It was ultimately found that, with this approach, the accelerations measured by the smartphones were very similar to those measured by the accelerometers.

When Eq. (5) was satisfied continuously for 0.2 s, the

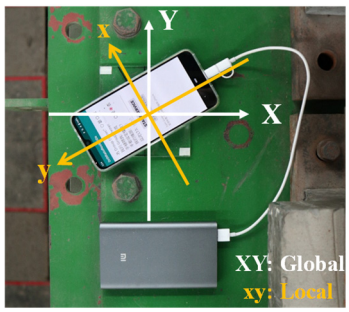

Fig. 17 The typical arrangement of the orientation of each smartphone on the fourth floor

smartphones were triggered, whereas when Eq. (6) was satisfied continuously for 1 s, they were de-triggered. The threshold in the equations was defined as the average value of the STA (μ_{STA}) plus four times the standard deviation of the STA (σ_{STA}) when the smartphones remained steady on the structure for 1 minute, as calculated using Eq. (7)

$$STA > 2LTA \quad \text{or} \quad STA > threshold \tag{5}$$

$$STA < LTA_{trigger} \quad \text{and} \quad STA < threshold \tag{6}$$

$$threshold = \mu_{STA} + 4\sigma_{STA} \tag{7}$$

It should be noted that there was a high level of hydraulic pressure in the actuators located under the shake table, such that some background vibration was induced in the structure even when a simulated earthquake excitation was not being applied. Moreover, the noise floor of this background vibration was very high, at approximately 5.0 cm/s^2. Such a high level of background vibration would not be typical during real-world applications, and this high background vibration made it difficult to trigger and de-trigger the smartphones during the tests, particularly during the small earthquakes. Furthermore, the large background vibration caused the earthquake classification function to be disabled during the experimental tests. Nonetheless, an electric shake table system was previously used to experimentally verify the performance of the earthquake classification function (Hsu and Nieh 2020).

The ground floor was successfully identified using the proposed approach. When the time was synchronized, the RMSE error and maximum absolute error of the best orientations using the Type II LFSD method were 4.2° and 12.5°, respectively. When the time was not synchronized, the RMSE error and maximum absolute error of the best orientations using the Type I LFSD method were 6.3° and 35.1°, respectively.

The effect of time synchronization and orientation alignment on the performance when using the CSI and FRF methods to estimate the lowest fundamental natural frequency is discussed next. The boxplots of the relative errors of the identified frequencies of the 14 earthquakes when using the CSI algorithm and the FRF algorithm are shown in Fig. 18. As shown in Fig. 18, the error when the time is synchronized and when using the CSI algorithm is always smaller than approximately 0.9%, either with or

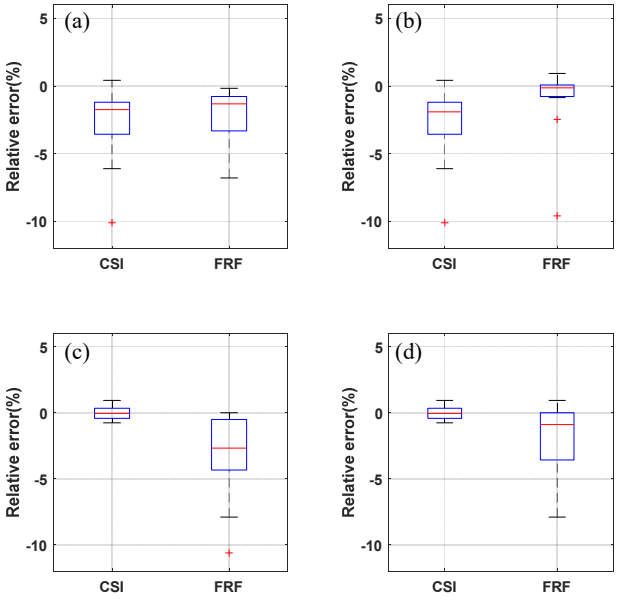

Fig. 18 The boxplots of the relative errors of the identified frequencies in the experimental study when (a) the smartphones are not aligned and the time is not synchronized; (b) the smartphones are aligned and the time is not synchronized; (c) the smartphones are not aligned and the time is synchronized; and (d) the smartphones are aligned and the time is synchronized

without the orientation alignment. However, if the time is not synchronized, the maximum relative error could reach approximately 10.1%. The results when using the CSI algorithm thus seem similar to the results in the numerical study, but in general the errors when using the CSI algorithm are smaller than the errors in the numerical study.

On the other hand, the maximum error when orientation alignment is not performed while using the FRF algorithm is approximately 10.6% when the time is synchronized, whereas the maximum error is approximately 6.8% when the time is not synchronized. When orientation alignment is performed, the maximum error when using the FRF algorithm is approximately 7.6% when the time is synchronized, whereas the maximum error is approximately 9.6% when the time is not synchronized. Comparing the results when using the FRF algorithm shown in Figs. 18(b) and (d), it is strange that many of the errors when the time is synchronized are even larger than the errors when the time is not synchronized. This occurs, however, because the intersection of the acceleration time histories measured on the different floors for the small earthquakes is too short due to the large noise from the shake table. Nevertheless, the error when using the FRF algorithm is quite small when orientation alignment is performed, even when the time is not synchronized.

5. Conclusions

This study proposed using crowdsourced smartphones distributed in a building to estimate the building's lowest fundamental natural frequency during an earthquake

excitation. Firstly, a preliminary study aimed at determining the feasibility of estimating a building's lowest fundamental natural frequency using crowdsourced smartphones was performed using a numerical model of a real building subjected to different earthquake excitations. Note that, originally, the information regarding the smartphones' orientations was not known. Moreover, whether or not the signal recording times of the smartphones are synchronized depends on whether or not the Wi-Fi Direct communication between adjacent smartphones is available.

The results of the numerical study indicated that the accuracy of the estimated lowest fundamental natural frequency when using either of the two output-only system identification algorithms, i.e., the SSI and FDD methods, is not acceptable, even when the time is perfectly synchronized and the orientation is correctly aligned.

In real-life situations, which crowdsourced smartphones are located on the ground floor of a building would not be known in advance. However, in order to employ input-output system identification algorithms during earthquake excitations, it is necessary to know which acceleration signals are measured by the smartphones located on the ground floor. The LFC algorithm is thus proposed in this study to determine which smartphones are on the ground floor or basement level based on the measured acceleration data. Based on the characteristic of the transmissibility between the ground input acceleration and the floor response acceleration, the algorithm determines that the floor with minimum frequency content with frequency smaller than 1.1 times that of the theoretical lowest fundamental natural frequency is the ground floor. The results indicated that the proposed algorithm can effectively identify which measured accelerations are the input ground excitations and should thus be used in the input-ouput system identification algorithms.

Based on the results of the numerical study, the Type II LFSD method is proposed to align the orientations of the accelerations measured by the smartphones on different floors when the time is synchronized based on the vibration signals measured, and the Type I LFSD method is proposed instead for those cases in which the time is not synchronized.

It is also found that the CSI algorithm is sensitive to time synchronization but not sensitive to orientation alignment; hence, if Wi-Fi Direct communication between adjacent smartphones is available, i.e., if the time is synchronized, it is suggested that the CSI algorithm be used to estimate the lowest fundamental natural frequency because of its high accuracy. On the other hand, the FRF algorithm is sensitive to orientation but not sensitive to synchronization; hence, it is recommended for estimating the lowest fundamental natural frequency when time synchronization is not available. It should further be noted that although error in orientation still exists even after orientation alignment is performed when using the LFSD methods, the accuracy of the estimated lowest fundamental natural frequency is acceptable when using the FRF algorithm.

The necessary algorithms including the trigger/de-trigger, earthquake classification, Wi-Fi Direct communication, and time synchronization algorithms were embedded in the smartphone application, and the proposed approach was verified using shake table tests of a scaled, four-story steel building. In general, the experimental study demonstrated that the accuracy of the estimated lowest fundamental natural frequency is quite acceptable when using the CSI and FRF algorithms when the time is synchronized and the orientation is aligned, respectively. However, when the time was synchronized, the errors of the estimated lowest fundamental natural frequency when using the FRF algorithm became larger than the errors produced in the numerical study. This occurred because the intersection of the acceleration time histories measured on the different floors for the small earthquakes was very short due to the large noise from the shake table.

Although the feasibility of using crowdsourced smartphone data to estimate the lowest fundamental natural frequencies of buildings during earthquakes has been illustrated based on the results of the numerical and experimental studies, it should be noted that this potential is actually based on some assumptions. First, the input excitation is assumed to be measured, because otherwise the input-output system identification algorithms cannot be employed. Therefore, in order to elevate the applicability of the proposed approach in practice, it is recommended that one fixed smartphone be deployed on the ground floor of a given building. It is also possible to use the accelerations measured by nearby seismic stations in the basement of a nearby building or in a nearby free field as the input, but more study is required to understand the feasibility of this approach. In addition, it is assumed that all the acceleration responses of each floor were measured. Relatedly, in the future, it is also worth studying cases in which the acceleration responses measured on only some floors are available.

It is also assumed that the crowdsourced smartphones are placed horizontally on the floor or on rigid pieces of furniture. The lowest natural frequency of firm furniture is relatively high, e.g., 10 Hz or higher, hence the lowest natural frequency of a building, e.g., approximately 5 Hz and lower, can possibly be identified without much difficulty. However, some of the smartphones could be placed on soft or unstable furniture, hence the identified the lowest natural frequency of a building could be affected. In addition, because in the practical application the smartphones are not fixed well on the floor, the smartphones could slide during earthquake excitations. The sliding effect is dependent on the surface of both the smartphones and the surface supporting the smartphone. When the smartphones slide during the earthquake excitation, identifying the lowest natural frequency of the structure could be affected. Kong *et al*. (2016b) found that the frequency content remained similar when the smartphones started to slide during shaking table tests of acceleration ~0.3g and above ~3 Hz. Hence the effect of identifying the lowest natural frequency of the structure may not be remarkable. However, further study is still required to clarify the effect. If the sliding effect is remarkable, one of the possible solutions is only using the signals smaller than 0.1 g because the static friction

coefficient of most of the cases is larger than 0.1. If only a few smartphones in a building are placed on soft or unstable furniture or are sliding during the earthquake excitations, using the outlier approach to exclude the data collected by these smartphones could be one of the possible solutions. Nevertheless, further studies should conducted to solve these problems.

Acknowledgments

This work was financially supported by the Taiwan Building Technology Center from The Featured Areas Research Center Program within the framework of the Higher Education Sprout Project by the Ministry of Education in Taiwan.

References

Borenius, S., Costa-Requena, J., Lehtonen, M. and Kantola, R. (2019), "Providing network time protocol based timing for smart grid measurement and control devices in 5G networks", *Proceedings of 2019 IEEE International Conference on Communications*, *Control*, *and Computing Technologies for Smart Grids* (*SmartGridComm*), Beijing, China, pp. 1-6.

Brincker, R., Zhang, L. and Andersen P. (2001), "Modal identification of output-only systems using frequency domain decomposition", *Smart Mater*. *Struct*., **10**(3), 441. https://doi.org/10.1088/0964-1726/10/3/303

Clayton, R.W., Heaton, T., Kohler, M., Chandy, M., Guy, R. and Bunn, J. (2015), "Community seismic network: A dense array to sense earthquake strong motion", *Seismol Res*. *Lett*., **86**(5), 1354-1363. https://doi.org/10.1785/0220150094

Dashti, S., Bray, J.D., Reilly, J., Glaser, S., Bayen, A. and Mari, E. (2014), "Evaluating the reliability of phones as seismic monitoring instruments", *Earthq Spectra*, **30**(2), 721-742. https://doi.org/10.1193/091711EQS229M

Dong, C.Z., Bas, S. and Catbas, F.N. (2019), "A completely non-contact recognition system for bridge unit influence line using portable cameras and computer vision", *Smart Struct*. *Syst*., *Int*. *J*., **24**(5), 617-630. https://doi.org/10.12989/sss.2019.24.5.617

Elhattab, A., Uddin, N. and Obrien, E. (2019), "Extraction of bridge fundamental frequencies utilizing a smartphone MEMS accelerometer", *Sensors*, **19**, 3143. https://doi.org/10.3390/s19143143

Ewins, D.J. (2000), *Modal Testing*, (2nd Ed.), Research Studies Press, Baldock.

Faulkner, M., Clayton, R., Heaton, T., Chandy, K.M., Kohler, M., Bunn, J., Guy, R., Liu, A., Olson, M., Cheng, M.H. and Krause, A. (2014), "Community sense and response systems: your phone as quake detector", *Commun*. *ACM*, **57**, 66-75. https://doi.org/10.1145/2622633

Feng, M., Fukuda, Y., Mizuta, M. and Ozer, E. (2015), "Citizen Sensors for SHM: Use of accelerometer data from smartphones", *Sensors*, **15**, 2980-2998. https://doi.org/10.3390/s150202980

Finazzi, F. (2016), "The earthquake network project: Toward a crowdsourced smartphone-based earthquake early warning system", *Bull*. *Seismol*. *Soc*. *Am*., **106**, 1088. https://doi.org/10.1785/0120150354

Finzi Neto, R.M., Steffen Jr, V., Rade, D.A., Gallo, C.A. and Palomino, L.V. (2010), "A low-cost electromechanical impedance-based SHM architecture for multiplexed piezoceramic actuators", *Struct*. *Health Monitor*., **10**, 391-402. https://doi.org/10.1177/1475921710379518

Haque, M.E., Zain, M.F.M., Hannan, M.A. and Rahman, M.H. (2015), "Building structural health monitoring using dense and sparse topology wireless sensor network", *Smart Struct*. *Syst*., *Int*. *J*., **16**(4), 607-621. https://doi.org/10.12989/sss.2015.16.4.607

Hsu, T.Y. and Nieh, C.P. (2020), "On-site earthquake early warning using smartphones", *Sensors*, **20**, 2928. https://doi.org/10.3390/s20102928

Hsu, T.Y., Yin, R.C. and Wu, Y.M. (2018), "Evaluating post-earthquake building safety using economical MEMS seismometers", *Sensors*, **18**(5), 1437. https://doi.org/10.3390/s18051437

Hsu, T.Y., Pham, Q.V., Chao, W.C. and Yang, T.S. (2020), "Post-earthquake building safety evaluation using consumer-grade surveillance cameras", *Smart Struct*. *Syst*., *Int*. *J*., **25**(5), 531-541. https://doi.org/10.12989/sss.2020.25.5.531

Hsu, T.Y., Liu, C.Y., Hsieh, Y.M. and Weng, C.T. (2022), "Post-earthquake fast building safety assessment using smartphone-based interstory drifts measurement", *Smart Struct*. *Syst*., *Int*. *J*., **29**(2), 287-299. https://doi.org/10.12989/sss.2022.29.2.287

Kim, R.E., Li, J., Spencer, B.F., Nagayama, T. and Mechitov, K.A. (2016a), "Synchronized sensing for wireless monitoring of large structures", *Smart Struct*. *Syst*., *Int*. *J*., **18**(5), 885-909. https://doi.org/10.12989/sss.2016.18.5.885

Kim, J.M., Han, M., Lim, H.J., Yang, S. and Sohn, H. (2016b), "Operation of battery-less and wireless sensor using magnetic resonance based wireless power transfer through concrete", *Smart Struct*. *Syst*., *Int*. *J*., **17**(4), 631-646. https://doi.org/10.12989/sss.2016.17.4.631

Kohler, M.D., Massari, A., Heaton, T.H., Kanamori, H., Hauksson, E., Guy, R., Clayton, R.W., Bunn, J. and Chandy, K.M. (2016), "Downtown Los Angeles 52-story high-rise and free-field response to an oil refinery explosion", *Earthq*. *Spectra*, **32**(3), 1793-1820. https://doi.org/10.1193/062315EQS101M

Kong, Q., Allen, R.M. and Schreier, L. (2016a), "Myshake: Initial observations from a global smartphone seismic network", *Geophys*. *Res*. *Lett*., **43**, 9588-9594. https://doi.org/10.1002/2016GL070955

Kong, Q., Allen, R.M., Schreier, L. and Kwon, Y.W. (2016b), "MyShake: A smartphone seismic network for earthquake early warning and beyond", *Sci*. *Adv*., **2**(2), e1501055. https://doi.org/10.1002/2016GL070955

Kong, Q., Allen, R.M., Kohler, M.D., Heaton, T.H. and Bunn, J. (2018), "Structural health monitoring of buildings using smartphone sensors", *Seismol*. *Res*. *Lett*., **89**, 594-602. https://doi.org/10.1785/0220170111

Lei, B., Ren, Y., Wang, N., Huo, L. and Song, G. (2020), "Design of a new low-cost unmanned aerial vehicle and vision-based concrete crack inspection method", *Struct*. *Health Monit*., **19**(6), 1871-1883. https://doi.org/10.1177/1475921719898862

Mills, D.L. (1991), "Internet time synchronization: the network time protocol", *IEEE Trans*. *Commun*., **39**(10), 1482-1493. https://doi.org/10.1109/26.103043

Miškinis, R., Smirnov, D., Urba, E. and Dzindzelėta, B. (2011), "Timing and synchronization in mobile telecommunication networks. Frequency Control and the European Frequency and Time Forum (FCS)", *Proceedings of 2011 Joint Conference of the IEEE International*, San Francisco, CA, USA, May, pp. 665-669.

Ozer, E., Feng, M.Q. and Feng, D. (2015), "Citizen sensors for SHM: Towards a crowdsourcing platform", *Sensors*, **15**, 14591-14614. https://doi.org/10.3390/s150614591

Peeters, B. and De Roeck, G. (1999), "Reference-based stochastic subspace identification for output-only modal analysis", *Mech*. *Syst*. *Signal Process*., **13**(6), 855-878. https://doi.org/10.1006/mssp.1999.1249

Reynders, E. and De Roeck, G. (2008), "Reference-based combined deterministic-stochastic subspace identification for experimental and operational modal analysis", *Mech. Syst. Signal Process.*, **22**(3), 617-637. https://doi.org/10.1016/j.ymssp.2007.09.004

Shen, Y., Fu, W., Luo, Y., Yun, C.B., Liu, D., Yang, P., Yang, G. and Zhou, G. (2021), "Implementation of SHM system for Hangzhou East Railway Station using a wireless sensor network", *Smart Struct. Syst., Int. J.*, **27**(1), 19-33. https://doi.org/10.12989/sss.2021.27.1.019

Shrestha, A., Dang, J. and Wang, X. (2018), "Development of a smart-device-based vibration measurement system: Effectiveness examination and application cases to existing structure", *Struct. Control Health Monit.*, **25**, e2120. https://doi.org/10.1002/stc.2120

Sun, Z., Krishnan, S., Hackmann, G., Yan, G., Dyke, S.J., Lu, C. and Irfanoglu, A. (2015), "Damage detection on a full-scale highway sign structure with a distributed wireless sensor network", *Smart Struct. Syst., Int. J.*, **16**(1), 223-242. https://doi.org/10.12989/sss.2015.16.1.223

Sun, K., Zhang, W., Ding, H., Kim, R.E. and Spencer, B.F. (2017), "Autonomous evaluation of ambient vibration of underground spaces induced by adjacent subway trains using high-sensitivity wireless smart sensors", *Smart Struct. Syst., Int. J.*, **19**(1), 1-10. https://doi.org/10.12989/sss.2017.19.1.001

Withers, M., Aster, R., Young, C., Beiriger, J., Harris, M., Moore, S. and Trujillo, J. (1998), "A comparison of select trigger algorithms for automated global seismic phase and event detection", *Bull. Seismol. Soc. Am.*, **88**(1), 95-106. https://doi.org/10.1785/BSSA0880010095

Wu, W.H, Wang, S.W., Chen, C.C. and Lai, G. (2017), "Assessment of environmental and nondestructive earthquake effects on modal parameters of an office building based on long-term vibration measurements", *Smart Mater. Struct.*, **26**, 055034. https://doi.org/10.1088/1361-665X/aa6ae6

Yu, Y., Han, R., Zhao, X., Mao, X., Hu, W., Jiao, D. and Ou, J. (2015), "Initial validation of mobile-structural health monitoring method using smartphones", *Int. J. Distrib. Sensor Networks*, **11**(2), p.274391. https://doi.org/10.1155/2015/274391

Yu, Q., Guan, B., Shang, T., Liu, X. and Li, Z. (2019), "Flexible camera series network for deformation measurement of large scale structures", *Smart Struct. Syst., Int. J.*, **24**(5), 587-595. https://doi.org/10.12989/sss.2019.24.5.587

Zonta, D., Wu, H., Pozzi M., Zanon, P., Ceriotti, M., Mottola, L., Picco, G.P., Murphy, A.L., Guna, S. and Corra, M. (2010), "Wireless sensor networks for permanent health monitoring of historic buildings", *Smart Struct. Syst., Int. J.*, **6**(5), 595-618. https://doi.org/10.12989/sss.2010.6.5_6.595